bioRxiv preprint doi: https://doi.org/10.1101/2020.01.25.919506; this version posted January 25, 2020. The copyright holder for this preprint (which was not certified by peer review) is the author/funder, who has granted bioRxiv a license to display the preprint in perpetuity. It is made available under aCC-BY 4.0 International license.

Heterozygous mutation of Sonic Hedgehog receptor (Ptch) drives cerebellar overgrowth and sex-specifically alters hippocampal and cortical layer structure, activity, and social behavior in female mice

Thomas W. Jackson, Gabriel A. Bendfeldt, Kelby A. Beam, Kylie D. Rock, Scott M. Belcher†

Center for Human Health and the Environment
Department of Biological Sciences
North Carolina State University
127 David Clark Labs Campus Box 7617
Raleigh, North Carolina, USA 27695-7617

Email address: Thomas Jackson: twjacks2@ncsu.edu
Gabriel Bendfeldt: gabendfe@ncsu.edu
Kelby Beam: kabeam2@ncsu.edu
Kylie Rock: kdrock@ncsu.edu
Scott Belcher: smbelch2@ncsu.edu

†***Corresponding author***: Scott M. Belcher, smbelch2@ncsu.edu

Funding: This work was supported in part by NIEHS training grant 5T32ES007046-38 and NIEHS grant P30ES025128.

Conflicts: The authors declare no conflicts of interest.

Abbreviations: ASD, Autism Spectrum Disorder; BCNS, Basal cell nevus syndrome; EGL, External germinal layer; ERβ, Estrogen receptor beta; GCPs, Granule cell precursors; HPE, holoprosencephaly; IGL, Internal granular layer; MB, medulloblastoma; ML, Molecular layer; mPFC, Medial prefrontal cortex; PL, Purkinje cell layer; Shh, Sonic hedgehog; ThN md and ThN vl, Thalamic mediodorsal and ventrolateral nuclei; VTA, Ventral tegmental area

bioRxiv preprint doi: https://doi.org/10.1101/2020.01.25.919506; this version posted January 25, 2020. The copyright holder for this preprint (which was not certified by peer review) is the author/funder, who has granted bioRxiv a license to display the preprint in perpetuity. It is made available under aCC-BY 4.0 International license.

Abstract

Sonic hedgehog (SHH) signaling is essential for the differentiation and migration of early stem cell populations during cerebellar development. Dysregulation of SHH-signaling can result in cerebellar overgrowth and the formation of the brain tumor medulloblastoma. Treatment for medulloblastoma is extremely aggressive and patients suffer life-long side effects including behavioral deficits. Considering that other behavioral disorders including autism spectrum disorders, holoprosencephaly, and basal cell nevus syndrome are known to present with cerebellar abnormalities, it is proposed that some behavioral abnormalities could be inherent to the medulloblastoma sequalae rather than treatment. Using a haploinsufficient SHH receptor knockout mouse model (*Ptch1*$^{+/-}$), a partner preference task was used to explore activity, social behavior and neuroanatomical changes resulting from dysregulated SHH signaling. Compared to wild-type, *Ptch1*$^{+/-}$ females displayed increased activity by traveling a greater distance in both open-field and partner preference tasks. Social behavior was also sex-specifically modified in *Ptch1*$^{+/-}$ females that interacted more with both novel and familiar animals in the partner preference task compared to same-sex wild-type controls. Haploinsufficency of PTCH resulted in cerebellar overgrowth in lobules IV/V and IX of both sexes, and female-specific decreases in hippocampal size and isocortical layer thickness. Taken together, neuroanatomical changes related to deficient SHH signaling may alter social behavior.

Key words: cerebellum, cortex, holoprosencephaly, hyperactivity, medial prefrontal cortex, medulloblastoma, sex differences.

bioRxiv preprint doi: https://doi.org/10.1101/2020.01.25.919506; this version posted January 25, 2020. The copyright holder for this preprint (which was not certified by peer review) is the author/funder, who has granted bioRxiv a license to display the preprint in perpetuity. It is made available under aCC-BY 4.0 International license.

1. Introduction

The cerebellum is a brain region important for coordinating control of voluntary motor movement, muscle tone, and balance (Altman and Bayer, 1997). Additionally, the cerebellum is involved in higher-order cognitive functions and related behaviors (Rogers et al., 2013a). Developmental cerebellar damage and abnormal cerebellar structure can result in impairment of motor function, cognition, and social reward behavior. Abnormalities of the prefrontal cortex, thalamus, and some cerebellar structures are a commonly observed feature of autism spectrum disorder (ASD). Emerging evidence supports the existence of behavioral circuits integrating the cerebellum, prefrontal cortex, and thalamus through dopaminergic signaling (Rogers et al., 2013a).

Normal cerebellar function depends on properly integrated actions of neurons residing in the three distinctive layers of the mature cerebellum: the molecular layer (ML), Purkinje cell layer (PL), and the internal granular layer (IGL). The ML is primarily comprised of synaptic interfaces between dendritic arbors of Purkinje cell neurons and the axonal parallel fibers of mature granule cells in the IGL. The PL is demarcated by a monolayer of Purkinje cell bodies that divide the ML from the IGL (Altman and Bayer, 1997). Granule cell precursors (GCPs) arise from a population of rhombic lip progenitors that migrate to the cerebellum and form the external germinal layer (EGL) where GCP proliferation continues until post-natal day 15 in mouse (Altman and Bayer, 1997). During the postnatal period of cerebellar development, the GCPs mitotically arrest, differentiate, and migrate through the ML and PL, and then reach their final destination in the IGL as mature granule cells. Development of the stereotypic structure of the cerebellum is a tightly regulated process that requires specific gradients of key morphogens (Martinez et al., 2013).

The Sonic Hedgehog (SHH) signaling pathway is necessary to induce differentiation and mitotic arrest of GCPs in the EGL, and subsequently acts to direct migration of the maturing granule cells to the IGL (Dahmane and Ruiz i Altaba, 1999). Those processes are mediated by

bioRxiv preprint doi: https://doi.org/10.1101/2020.01.25.919506; this version posted January 25, 2020. The copyright holder for this preprint (which was not certified by peer review) is the author/funder, who has granted bioRxiv a license to display the preprint in perpetuity. It is made available under aCC-BY 4.0 International license.

the morphogen SHH which binds to the Patched-1 (PTCH1) receptor expressed in Purkinje cells, GCPs, and cerebellar interneurons. Secretion of SHH from Purkinje cells is initiated around E17.5 in the mouse and peaks around postnatal day 6-8. The resulting SHH concentration gradient regulates differentiation of GCPs wherein lower concentrations of the morphogen allow continued proliferation. In the absence of the SHH ligand, PTCH1 inhibits Smoothened (SMO), a downstream G-protein coupled receptor. By contrast, SHH binding leads to disinhibition of SMO, resulting in increased activation of glioma-associated oncogene homolog (GLI) transcription factors. Uncontrolled disinhibition of SMO can result in failure of GCPs to differentiate, resulting in continued and excessive GCP proliferation, thereby overpopulating the IGL (Goodrich et al., 1997).

Mutations of genes encoding SHH pathway proteins are implicated in several human neurodevelopmental disorders (Hahn et al., 1996). Holoprosencephaly (HPE), most frequently caused by mutations of SHH, are the most common congenital forebrain abnormality in humans (Nanni et al., 1999; Solomon et al., 2010; Weiss et al., 2018a). Less commonly, mutations of PTCH1, the receptor for SHH, are also associated with HPE (Ming et al., 2002). Patients with HPE present with a wide array of phenotypes including forebrain malformations, craniofacial defects, and behavioral abnormalities including attention deficit hyperactivity disorder (ADHD) (Croen et al., 1996; Heussler et al., 2002).

Mutations of PTCH1 causing dysregulation of SHH are also associated with basal cell nevus syndrome (BCNS) (Gloude et al., 2016; Okamoto et al., 2014). Some BCNS patients develop skeletal anomalies, and approximately 3% develop the cerebellar brain cancer medulloblastoma (MB) (Lacombe et al., 1990). Molecular characterization of MB tumors has revealed that that 20-30% of MB patients have mutations in the SHH pathway (Northcott et al., 2012). The role of dysregulated SHH signaling in MB has been experimentally demonstrated using genetically modified strains of mice containing constitutively active Smo alleles, or knockout mutations of Ptch, that result in aberrant GLI1 transcriptional activity that gives rise to MB (Dey et al., 2012;

bioRxiv preprint doi: https://doi.org/10.1101/2020.01.25.919506; this version posted January 25, 2020. The copyright holder for this preprint (which was not certified by peer review) is the author/funder, who has granted bioRxiv a license to display the preprint in perpetuity. It is made available under aCC-BY 4.0 International license.

Goodrich et al., 1997; Grammel et al., 2012; Hallahan et al., 2004; Lee et al., 2007; Schüller et al., 2008; Uziel, 2005; Wetmore et al., 2001). Ptch1-knockout mice, initially developed to evaluate the role of the SHH-PTCH signaling pathway in BCNS, have been used widely to study MB (Goodrich et al., 1997; Nitzki et al., 2012). Whereas homozygous knockout of the PTCH1 receptor gene (*Ptch1*$^{-/-}$) is embryonically lethal due to failures of neural tube closure, haploinsufficient *Ptch* heterozygous mice (*Ptch1*$^{+/-}$) are viable but have increased SMO and GLI1 activity resulting from decreased PTCH1 protein expression (Goodrich et al., 1997). Phenotypically, that dysregulation of GLI1 transcriptional programming results in increased GCP proliferation, aberrant neuronal migration, and MB in 10-20% of *Ptch1*$^{+/-}$ adult mice (Zurawel et al., 2000). In addition to cerebellar dysregulation and MB tumorigenesis, altered hippocampal structures have been reported in male *Ptch1*$^{+/-}$ adult mice (Antonelli et al., 2018). A finding consistent with SHH signaling also having potential roles in neurogenesis of hippocampal progenitors hippocampal (Yao et al., 2016).

As was observed in experimental mouse models, mutations in humans causing unregulated activation of SHH-signaling, either via gain of SMO or loss of PTCH function, also result in MB. Medulloblastoma are one of the most common solid tumors of childhood, accounting for approximately 20% of all pediatric tumors. There are noted sex differences in some molecular subgroups of MB, with overall incidence showing a 1.5:1 male to female sex ratio; however, the sex ratio differs by population and depends on the etiology of the tumor (Northcott et al., 2012; Sun et al., 2015). The WNT and SHH subgroups of MB present with a 1:1 sex ratio (Northcott et al., 2012). Estrogen receptor β (ERβ) is expressed in maturing GCPs and MB tumor cells and can modify MB growth and progression (Belcher, 2008; Jakab et al., 2001). Increased estrogen receptor signaling during cerebellar development and MB progression results in upregulation of cytoprotective ERβ-dependent insulin-like growth factor signaling that impacts GCP maturation

bioRxiv preprint doi: https://doi.org/10.1101/2020.01.25.919506; this version posted January 25, 2020. The copyright holder for this preprint (which was not certified by peer review) is the author/funder, who has granted bioRxiv a license to display the preprint in perpetuity. It is made available under aCC-BY 4.0 International license.

and migration, and can increase MB tumor growth rate (Belcher, 2008; Cookman and Belcher, 2015).

Clinical treatment for MB is extremely aggressive and associated with severe life-long side effects in survivors. Typical treatment for MB involves primary tumor resection followed by radiation therapy and cytotoxic chemotherapy. Neurological complications including impaired attention and processing speed, learning and memory, language, visual perception, and executive functions occur in nearly all MB survivors and cause difficulties with social functions that can greatly decrease quality of life (Ribi et al., 2005). While associated with treatment, these behavioral defects and cognitive deficits resemble the hallmark behavioral symptoms associated with HPE and BCNS. The neurological deficits in MB survivors have been solely attributed to therapeutic side effects, but some component of the behavioral deficits in patients with MB may result from IGL overgrowth inherent to the SHH MB sequalae. To determine whether heterozygous mutation of *Ptch1* alone may influence behavior, male and female *Ptch1*$^{+/-}$ mice and their wildtype littermates were assayed using several behavioral tasks. Following behavioral analysis, brains from these *Ptch1*$^{+/-}$ mice were examined histologically to identify neuroanatomical alterations in structures potentially related to cerebello-cortical circuitry that could influence social behavior.

bioRxiv preprint doi: https://doi.org/10.1101/2020.01.25.919506; this version posted January 25, 2020. The copyright holder for this preprint (which was not certified by peer review) is the author/funder, who has granted bioRxiv a license to display the preprint in perpetuity. It is made available under aCC-BY 4.0 International license.

2. Experimental Procedures

2.1. *Animal Husbandry*

All animal procedures and reporting adhere to the ARRIVE guidelines (Supplemental data) and were performed in accordance with protocols approved by the North Carolina State University (NCSU) Institutional Animal Care and Use Committee following recommendations of the Panel on Euthanasia of the American Veterinary Medical Association. Study animals were housed on a 12:12 light cycle at 25°C and 45%-60% average relative humidity in an AAALAC accredited animal facility. Mice were housed in thoroughly washed polysulfone cages with woodchip bedding and pulped virgin cotton fiber nestlets (Ancare, Bellmore, NY). Soy-free Teklad 2020X diet (Envigo, Madison, WI) was supplied *ad libitum*. Sterile drinking water produced from a reverse osmosis water purification system (Millipore Rios with ELIX UV/Progard 2, Billerica, MA) was supplied *ad libitum* from glass water bottles with rubber stoppers and metal sippers.

Strains C57Bl6/J and STOCK *Ptch1*^{tm1Mps}/J were obtained from Jackson Laboratory (Bar Harbor, ME). Breeding was performed in-house to propagate both lines. Heterozygote *Ptch1* mutants and wildtype littermates were used for experimental procedures. Adult mice that presented with MB tumors were excluded from analyses. Genomic DNA was isolated from a 5 mm tail biopsy using a rapid digestion method where 95 μl of lysis buffer reagent (Viagen Biotech, Los Angeles, CA; Cat: 102-T) and 5 μl of Proteinase K (20 mg/ml; Viagen Biotech, Los Angeles, CA; Cat: 501-PK) were added to the biopsy sample, incubated for 4 hours at 55°C and 45 minutes at 85°C. Isolated DNA was used to identify offspring genotype following recommended genotyping protocol (Jax, Bar Harbor, ME) and analyzed by agarose gel electrophoresis on 1.5% gels. Heterozygotes were identified by the presence of both wild-type (200 base pair) and mutant (479 base pair) specific PCR products. Mice were weaned on postnatal day 21 (PND 21), assigned a coded identification number (Supplemental Table 1),

bioRxiv preprint doi: https://doi.org/10.1101/2020.01.25.919506; this version posted January 25, 2020. The copyright holder for this preprint (which was not certified by peer review) is the author/funder, who has granted bioRxiv a license to display the preprint in perpetuity. It is made available under aCC-BY 4.0 International license.

and identified by ear notching. No notable pathology differences or morbidity were detected in *Ptch1*$^{+/-}$ mice aside from development of MB in a subset of animals (18% of female; 9% of male) that were excluded from analyses due to death or ataxia associated with MB-like tumors detected at necropsy.

2.2. *Behavior Tests and Analysis*

All behavioral testing was conducted in a dedicated behavioral testing room at the NCSU Biological Resources Facility. Mice were transported in their home cage to the testing room on a covered rolling cart and tested after a minimum 30-minute acclimation period. Animals were tested in the last three hours of the light cycle. Both novel social and partner preference tasks used a blue, opaque arena (58 cm x 58 cm) with four high walls (43 cm). All arenas were in the same room with two conspecific animals run concurrently. Each animal was gently placed in the middle of the arena and given 30 minutes to explore, during which time they were not disturbed. No observer was present in the room. Behavioral data was digitally recorded (Handycam HDR-CX190, Sony, Tokyo) and automatically scored using TopScan behavioral analysis software (CleverSys, Inc, Reston, VA). For analysis, the floor of the open field arena was digitally divided into a 3x3 square grid, creating 9 squares in total of equal size. The middle square was designated as the center. All data was collected and analyzed by observers blinded to experimental group, and were validated by hand-scoring using a stop-watch.

2.2.1. *Novel Social Task*

Adult mice (wild-type: mean age: PND96, range: PND75-114; *Ptch1*$^{+/-}$ mean age: PND99; range: PND75-119) were tested for 30 minutes in the novel social arena as described previously (Winslow, 2003). A naïve same sex and younger/smaller, unrelated wild-type stimulus animal was caged in a randomly selected corner of the arena. The first five minutes of the trial were excluded from analyses to account for increased exploratory behavior that is commonly observed during entry into a novel environment (Bailey and Crawley, 2009). Maximum velocity and distance traveled were used to examine motor function decrements.

bioRxiv preprint doi: https://doi.org/10.1101/2020.01.25.919506; this version posted January 25, 2020. The copyright holder for this preprint (which was not certified by peer review) is the author/funder, who has granted bioRxiv a license to display the preprint in perpetuity. It is made available under aCC-BY 4.0 International license.

Center crosses, time spent along the wall, number of interactions, and time spent interacting were used to assess sociability. Latency to enter the stimulus animal's area, frequency of movement within areas of the arena, number of contact bouts, and duration within stimulus animal's area and exploratory areas were analyzed.

2.2.2. *Partner Preference Task*

Twenty-four hours after the novel social testing, animals were tested with two same-sex conspecific wild-type animals to examine the effects of *Ptch1* haploinsufficiency on social interaction and formation of partner preference (Winslow, 2003). Briefly, the same stimulus animal used for the novel social task was caged in one corner as a now-familiar animal, while a novel unfamiliar mouse was caged in the opposite corner. Latency to enter each stimulus animal's area, frequency of movement within areas of the arena, number of contact bouts with each animal, and duration within stimulus animal's area and exploratory areas were analyzed.

2.2.3 Olfactory *Task*

The ability of a subset of experimental animals to respond to a desirable olfactory cue was evaluated using an established protocol to assess intact recognition of a food-reward smell (Yang and Crawley, 2009). Briefly, animals were fasted for 12 hours overnight with *ad libitum* access to water and then placed into a clean cage containing a single previously buried Apple Jack (Kellogg, Battle Creek); the time required to locate and pick up the Apple Jack was measured using a stopwatch. An a priori maximum latency threshold of >900 seconds for food-treat discovery was defined as indicative of a decrement responsiveness (Yang and Crawley, 2009).

2.3. Neuroanatomy and Histology

Following completion of behavioral testing mice were euthanized by CO_2 asphyxiation. Brains were isolated by dissection, rapidly frozen on powdered dry ice, and stored at -80^{o}C until prepared for analysis. Brains and cerebella were separately embedded in OCT (Fisher Scientific, Hampton, NH) and mounted directly onto cryostat chucks for cryosectioning. Serial

bioRxiv preprint doi: https://doi.org/10.1101/2020.01.25.919506; this version posted January 25, 2020. The copyright holder for this preprint (which was not certified by peer review) is the author/funder, who has granted bioRxiv a license to display the preprint in perpetuity. It is made available under aCC-BY 4.0 International license.

mid-sagittal cryosections (20 μm) from the central vermis of each cerebellum and serial coronal cryosections (40 μm) of the brain were sectioned using a Leica Cryostat (Leica CM1900, Nussloch, Germany), mounted onto Superfrost plus slides (Fisher Scientific, Pittsburgh, PA), and stored at -80^{o}C until histological processing.

For Nissl staining, sections were brought to room temperature and immersed in xylene (Fisher Scientific, Hampton, NH; Cat: X5-500) for 30 minutes, 100% ethanol (Fisher Scientific, Hampton, NH; Cat: 22-032-601) for 3 minutes, 95% ethanol for 3 minutes, and Milli-Q water for 2 minutes before staining with 0.2% Cresyl Violet (Fisher Scientific, Hampton, NH; Cat: AC405760025) for 12 minutes. Sections were then dehydrated by immersing in 95% ethanol for 30 seconds, 100% ethanol for 30 seconds, and 3 washes in Xylene for 1 minute each. Slides were then cover-slipped using Permount (Electron Microscopy Sciences, Hatfield, PA; Cat: 17986-01).

Stained sections were examined by an investigator blind to genotype and sex on a Nikon Eclipse 80i microscope using a DSFi1 CCD camera controlled with Digital Sight software (Nikon; Melville, NY). Digital bright field micrographs of sections from the most medial 100-microns of the vermis were collected using the 2x objective for analysis of cerebellar morphology. For IGL area quantification, the most medial 20-micron section was defined using consecutive serial sections and identified by using the following criteria: the 4th ventricle protrudes towards lobule IX, deep cerebellar nuclei (fastigial nucleus, interposed nucleus, and dentate nucleus) are absent, and lobule X had a distinct nodulus. Coronal 40-micron cryosections of the cortex were assessed for gross morphometric differences at each of the following three landmarks. The first region was identified using the following criteria: ammon's horn extends through the section, supramammilary and medial mammillary nuclei were present, and nucleus of Darkschewitsch was present (Bregma -2.88). The second region was identified using the following criteria: the 3rd ventricle extends through section and arcuate nucleus was

bioRxiv preprint doi: https://doi.org/10.1101/2020.01.25.919506; this version posted January 25, 2020. The copyright holder for this preprint (which was not certified by peer review) is the author/funder, who has granted bioRxiv a license to display the preprint in perpetuity. It is made available under aCC-BY 4.0 International license.

present; (Bregma -1.755). The third region was identified using the following criteria: CA3 appears circular, lateral ventricle is rhomboid with a tail (Bregma -1.06). Digital bright field micrographs were collected using 1x and 2x Nikon objectives (Nikon, Tokyo, Japan; Cat: MRL00012 and MRL00022) and compared to a standardized atlas to identify gross morphometric differences. (Allen Institute for Brain Science, 2011, Seattle, WA). Areas of interest were measured using Nikon NIS Elements AR 3.2 with final figures of representative sections generated using Adobe Photoshop (San Jose, CA).

2.4. *Statistical Analysis*

Data analysis was performed using a 2-way (sex, genotype) or 3-way (sex, genotype, novelty/sociality/5-min period) multivariate analysis of variance as indicated. For analysis of cerebellar lobules and cortical layers, data analysis was performed using repeated measure ANOVA. Litter was included as a covariate and adjusted for if necessary. All animal assignments and litter information are provided (Supplemental Table 1). If overall effects were significant, a Fisher's least significant differences post hoc test was performed to evaluate pair-wise differences. For neuroanatomical endpoints, confounds related to possible litter effects were avoided by limiting analysis to one animal of a given sex from each litter. A minimal level of statistical significance for differences in values among or between groups was considered $p < .05$. Percentage data was arcsine transformed (arcsine of the square root of the percentage) prior to statistical analysis. All data were analyzed using GraphPad Prism v8 (GraphPad; La Jolla, CA) or SPSS v26 (IBM, Armonk, NY).

bioRxiv preprint doi: https://doi.org/10.1101/2020.01.25.919506; this version posted January 25, 2020. The copyright holder for this preprint (which was not certified by peer review) is the author/funder, who has granted bioRxiv a license to display the preprint in perpetuity. It is made available under aCC-BY 4.0 International license.

3. Results

3.1. General locomotor function and exploratory behavior

Since the cerebellum is critical in motor function, general locomotor function was assessed during the open-field novel social task to evaluate whether *Ptch1*$^{+/-}$ mice exhibit motor deficits. Multivariate analysis of variance (MANOVA) showed no deficits in maximum velocity over the 30-minute trial ($F(1, 68) = .14$, $p = .71$) (Figure 1A). Multivariate analysis of variance showed an interaction of sex and genotype on total distance traveled ($F(1, 54 = 4.52$, $p = .04$, $\eta 2 = .55$)). Post hoc analysis using Fisher's LSD indicated that total distance traveled by *Ptch1*$^{+/-}$ females only was increased compared to wild-type (females: $p = .009$; males: $p = .84$) (Figure 1B). Repeated measures 3-way MANOVA with sex (male, female) as the within-subjects factor, 5-min period (1-6), and genotype (wild-type, *Ptch1*$^{+/-}$) as the between-subjects factors revealed a significant interaction of sex and genotype on distance traveled across 5-minute periods ($F(1, 53 = 4.28$, $p = .04$, $\eta 2 = .18$)). A follow-up repeated measures 2-way MANOVA within sex revealed that females only were significantly different in distance traveled across 5-minute periods (females: $p = .002$; male: $p = .47$) (Figure 1C and 1D).

During the open-field novel social task, time spent along the wall and number of center crosses over the 30-minute trial were assessed to examine exploratory behavior. Multivariate analysis of variance showed no differences in time spent along the wall ($F(1, 68 = .79$, $p = .38$)) (Supplemental Figure 1). Consistent with increased distance traveled, MANOVA found a significant effect of genotype on center crosses ($F(1, 68 = 8.47$, $p = .006$, $\eta 2 = .81$)) (Supplemental Figure 1). Post hoc analysis using Fisher's LSD indicated a significant increase in number of center crosses in *Ptch1*$^{+/-}$ females only (females: $p = .02$; males: $p = .55$). In the novel social task, MANOVA found no differences in the number of interactions ($F(1, 68 = 1.98$, $p = .16$) or the duration of those interactions ($F(1, 68 = 0.20$, $p = .66$) with the novel animal.

bioRxiv preprint doi: https://doi.org/10.1101/2020.01.25.919506; this version posted January 25, 2020. The copyright holder for this preprint (which was not certified by peer review) is the author/funder, who has granted bioRxiv a license to display the preprint in perpetuity. It is made available under aCC-BY 4.0 International license.

3.2. Social behavior

To assess the effects of *Ptch1* mutation on social behavior, a partner preference task was used. As in the novel social task, MANOVA of the partner preference task showed no differences in maximum velocity (F(1, 57 = .59, p = .45) (Figure 1A) nor time spent along the wall (F(1, 57 = 3.72, p = .06)) (Supplemental Figure 2). In the partner preference task, MANOVA again detected a significant interaction between sex and genotype on total distance traveled (F(1, 56 = 4.12, p = .048, η2 = .51). Post hoc analysis using Fisher's LSD identified a significant increase in total distance traveled was again in *Ptch1*$^{+/-}$ females only (females: p = .002; males: p = .71). Multivariate analysis of variance again showed a main effect of genotype on center crosses consistent with increased distance traveled (F(1, 57 = 5.99, p = .02, η2 = .67)) (Supplemental Figure 2). Post hoc analysis using Fisher's LSD identified a significant increase in total distance traveled was again in *Ptch1*$^{+/-}$ females only (females: p = .02; males: p = .22).

A 3-way MANOVA with sex (male, female) as the within-subjects factor, and novelty (novel, familiar) and genotype (wild-type, *Ptch1*$^{+/-}$) as the between-subjects factors, revealed an interaction between sex and genotype on the duration of interactions during the partner preference task (F(1, 110) = 8.59, p = .005, η2 = .82)). Post hoc analysis using Fisher's LSD revealed that *Ptch1*$^{+/-}$ females only show increased time spent interacting with both novel (females: p = .047; males: p = .72) and familiar animals (females: p = .03; males: p = .93) (Figure 2A). All other main effects were non-significant and not relevant to the tested hypotheses.

A 3-way MANOVA with sex (male, female) as the within-subjects factor and novelty (novel, familiar) and genotype (wild-type, *Ptch1*$^{+/-}$) as the between-subjects factors revealed an interaction between sex and genotype on the number of interactions during partner preference task (F(1, 111) = 14.52, p = .0002, η2 = .22)). That interaction was qualified by an interaction between novelty, sex, and genotype (F(1, 111) = 7.698, p = .007, η2 = .11)). Post hoc analysis using Fisher's LSD revealed that *Ptch1*$^{+/-}$ females only show an increase in the number of

bioRxiv preprint doi: https://doi.org/10.1101/2020.01.25.919506; this version posted January 25, 2020. The copyright holder for this preprint (which was not certified by peer review) is the author/funder, who has granted bioRxiv a license to display the preprint in perpetuity. It is made available under aCC-BY 4.0 International license.

interactions with the novel animal (females: $p < .0001$; males: $p = .10$) (Figure 2B). All other main effects were non-significant and not relevant to the tested hypotheses.

A 3-way ANOVA with sex (male, female) as the within-subjects factor, and sociality (nose-nose, nose-tail) and genotype (wild-type, *Ptch1*$^{+/-}$) as the between-subjects factors, revealed a significant interaction between sex, sociality, and genotype on the percentage of nose-tail bouts ($F(1, 136) = 7.24$, $p = .01$, $\eta 2 = .75$). Post hoc analysis using Fisher's LSD revealed that *Ptch1*$^{+/-}$ females only show increased nose-tail bouts relative to wild-type (females: $p = .0003$; males: $p = .81$) (Figure 2C). All other main effects were non-significant and not relevant to the tested hypotheses.

3.3. *Olfaction*

The ability of test animals to respond to a desirable food-treat was evaluated to ensure that modifications in social behaviors were not influenced by unanticipated decrements in ability to identify and respond to olfactory cues or a lack of motivation. A subset of wild-type (female: n=7; male: n=5) and *Ptch1*$^{+/-}$ (female: n=3; male: n=2) were evaluated using an established protocol to assess intact recognition of smell wherein a latency greater than 15 minutes (900 seconds) is considered indicative of a decrement in smell (Yang and Crawley, 2009). There were no test failures with all animals tested rapidly discovering the olfactory stimulus in less than the allotted task time. The maximum time for any animal to complete the task was less than 4 minutes (231 seconds).

3.4. Cerebellar and cortical structures

In contrast to the stereotypic morphology of the cerebellum observed in both male and female wild-type mice (Figure 3A and 3C), granule cell overgrowth with localized thickening of the IGL was commonly observed in the *Ptch1*$^{+/-}$ mutants (Figure 3B and 3D; asterisks). Ectopic granule cells were also observed in 43% (6/14) of *Ptch1*$^{+/-}$ females (Figure 3B; arrow) and 45% (5/11) of *Ptch1*$^{+/-}$ males, compared to vermis of the cerebellum from wild-type mice (Figure 3A,

bioRxiv preprint doi: https://doi.org/10.1101/2020.01.25.919506; this version posted January 25, 2020. The copyright holder for this preprint (which was not certified by peer review) is the author/funder, who has granted bioRxiv a license to display the preprint in perpetuity. It is made available under aCC-BY 4.0 International license.

344 female; 3C, male) where ectopic granule cells were not observed in either sex (female: n=9;
345 male: n=9).

346 The extent of granule cell overgrowth was assessed by quantitative comparison of IGL
347 area in the cerebellar vermis of wildtype and *Ptch1*$^{+/-}$ mutants. Repeated measures analysis of
348 variance showed a significant effect of genotype on total IGL area ($F(1, 31 = 7.349$, $p = .01$, $\eta 2$
349 $= .99$)). Post hoc analysis for total IGL area using Fisher's LSD was not statistically significant in
350 either sex (Figure 3B; female: $p = .06$; male: $p = .07$), but differences in the area of individual
351 lobules of the cerebellum appeared to drive the detected effect of genotype (Table 1; Figure
352 3E). Repeated measures ANOVA for the IGL area of individual lobules detected a significant
353 main effect of genotype on IGL area ($F(1, 31 = 13.7$, $p = .002$, $\eta 2 = .98$) with post hoc analysis
354 using Fisher's LSD demonstrating specific effects in both sexes on lobules IV/V (females: $p =$
355 .02; males: $p = .001$), VII (females: $p = .04$; males: $p = .009$), VIII (females: $p = .046$; males: $p =$
356 .008), and IX (females: $p = .001$; males: $p = .01$) and in males only in lobule VI (females: $p =$
357 .82; males: $p = .001$) (Figure 3E). Overt loss of Purkinje cells or differences in the width of the
358 Purkinje cell monolayer were not observed in the cerebellum of either sex.

359 Outside of the cerebellum, malignancy or gross morphological changes in the brains of the
360 *Ptch*$^{+/-}$ mutants were not observed. To evaluate potential structural differences in the extra-
361 cerebellar brain regions of *Ptch1*$^{+/-}$ mutants, hippocampal and cortical structures implicated in
362 playing a functional role in cerebellar functions and related behaviors were compared. Analysis
363 of variance of the length of ammon's horn (Figure 4A-4C) showed a statistically significant
364 interaction of genotype and sex ($F(1, 14 = 4.62$, $p = .0495$, $\eta 2 = .39$). Post hoc analysis using
365 Fisher's LSD indicated that this hippocampal structure in *Ptch1*$^{+/-}$ females only was significantly
366 smaller than wildtype (females: $p = .006$; males: $p = .75$) (Figure 4D). Analysis of variance of the
367 dentate gyrus length showed a statistically significant interaction of genotype and sex ($F(1, 14 =$
368 7.16, $p = .02$, $\eta 2 = .40$)). Post hoc analysis using Fisher's LSD indicated that the dentate gyrus
369 of *Ptch1*$^{+/-}$ females only was similarly reduced in size compared to wild-type (females: $p = .006$;

bioRxiv preprint doi: https://doi.org/10.1101/2020.01.25.919506; this version posted January 25, 2020. The copyright holder for this preprint (which was not certified by peer review) is the author/funder, who has granted bioRxiv a license to display the preprint in perpetuity. It is made available under aCC-BY 4.0 International license.

370 males: p = .71) (Figure 4D). Lateral ventricle area was measured because of noted differences
371 of the lateral ventricle in BCNS syndrome and ASD (Shiohama et al., 2017; Turner et al., 2016).
372 Analysis of variance showed no differences in lateral ventricle area ($F(1, 11 = 0.93$, $p = .35$)).
373 In the cortex, a main effect of genotype on overall cortical layer length ($F(1, 14 = 6.24$, $p =$
374 $.03$, $\eta 2 = .80$)) was detected, however post hoc analysis of total cortical layer length (Figure 4A)
375 was not statistically significant for either sex (female: p = .10; male: p = .10). Analysis of
376 variance of overall cortical layer width showed no effect from sex or genotype ($F(1, 14 = 1.65$, p
377 $= .22$). However, increased cellularity in all cortical layers was observed in *Ptch1*$^{+/-}$ females
378 (Figures 4B; 4C). Repeated measures ANOVA found a significant effect of genotype on the
379 width of individual cortical layers ($F(1, 25) = 8.2$, $p = .02$, $\eta 2 = .48$). Post hoc analysis using
380 Fisher's LSD detected specific effects in lobule VI in females only (females: p = .007; males: p =
381 .35) (Figure 4E). No effect of sex or genotype was detected in either sex in cortical layers I
382 (females: p = .22; males: p = .65)), II/III/IV (females: p = .09; males: p = .70)) or V (females: p
383 =.14; males: p = .20).

bioRxiv preprint doi: https://doi.org/10.1101/2020.01.25.919506; this version posted January 25, 2020. The copyright holder for this preprint (which was not certified by peer review) is the author/funder, who has granted bioRxiv a license to display the preprint in perpetuity. It is made available under aCC-BY 4.0 International license.

4. Discussion

4.1. *Sex-specific alterations of social behavior and activity of Ptch1*$^{+/-}$ females

Dysregulation of SHH signaling resulted in a significant interaction of sex and genotype that drove the female-specific social behavioral effects observed in the novel open-field and partner preference tasks. *Ptch1*$^{+/-}$ females traveled further and had more center crosses in both the novel open-field and partner preference tasks. In the partner preference task, *Ptch1*$^{+/-}$ females spent increased time with both novel and familiar animals and had increased nose-tail interactions relative to wild-type mice. In mice, most novel social interactions involve nose-nose contact, this investigative social activity contrasts with aggressive nose-tail interactions (Silverman et al., 2010). There were no detected differences in the type or duration of social behavior displayed in the male *Ptch1*$^{+/-}$ mutants. Prosocial phenotypes observed in *Ptch1*$^{+/-}$ females indicated differential responsiveness to dysregulated SHH signaling wherein female sex exacerbates alterations in social behavior and hyperactivity.

Because the *Ptch* knockout mutation used in this study resulted in global deficits of PTCH, pleiotropic effects from *Ptch1* haploinsufficiency could have contributed to the observed behavioral changes. The cerebellum is critical in motor movement (Altman and Bayer, 1997), and disrupted SHH signaling has been linked to changes in olfactory neuron production (Daynac et al., 2016; Gomez et al., 2019; Ihrie et al., 2011; Tong et al., 2015). To rule out trivial explanations for altered behaviors observed, we carefully assessed movement in our novel open-field task for evidence of decrements related to compromises mechano-skeletal ability, cerebellar control of coordination or movement, and to rule out defects related to olfaction. No deficits in movement velocity, distance traveled, or latency to find an olfaction cue were detected. In fact, there was a paradoxical increase in the activity of *Ptch1*$^{+/-}$ females indicated by increases in total distance moved. Sustained activity after the first five minutes indicates a failure of *Ptch1*$^{+/-}$ females to acclimate to the arena (Figure 1C), suggesting more complicated

bioRxiv preprint doi: https://doi.org/10.1101/2020.01.25.919506; this version posted January 25, 2020. The copyright holder for this preprint (which was not certified by peer review) is the author/funder, who has granted bioRxiv a license to display the preprint in perpetuity. It is made available under aCC-BY 4.0 International license.

409 sex-specific impacts than decreased movement coordination or loss of the ability to smell were
410 responsible for the observed alterations in behavior.

411 Increased activity and prosocial behaviors of *Ptch1*$^{+/-}$ females could be explained by a
412 hyperactivity phenotype. In humans, ADHD has been associated with HPE caused by SHH
413 mutations primarily in female humans with noted high intellectual function (Heussler et al., 2002;
414 Solomon et al., 2012), demonstrating that altered SHH signaling can lead to hyperactivity.
415 Similar to the sex differences observed in *Ptch1*$^{+/-}$ female mice, human females are also at
416 increased risk for diagnosis of HPE with sex ratios ranging from 1.2:1 to 2.3:1 female:male
417 (Croen et al., 1996; Mouden et al., 2016; Weiss et al., 2018a). The prosocial phenotype
418 observed in *Ptch1*$^{+/-}$ females may be due to a mild sex-specific HPE-like hyperactive phenotype
419 resulting in indiscriminate social interactions.

420 *4.2. Neuroanatomical examination of cerebellar structure*

421 The presented findings from behavioral tasks supplement previous work demonstrating
422 that haploinsufficiency of Ptch1 can alter cognitive behaviors including reduced motor learning
423 ability and performance on a spatial memory task by linking dysregulation of SHH signaling with
424 hyperactivity and altered social behaviors (Antonelli et al., 2018; Dutka et al., 2015). The altered
425 social behavior in *Ptch1*$^{+/-}$ females may be related to cerebellar overgrowth, which is
426 increasingly appreciated for its role in schizophrenia, dementia, and other psychiatric disorders
427 (Phillips et al., 2015).

428 Imaging, clinical, and experimental animal studies have linked the cerebellum with
429 cognitive brain disorders including ASD and BCNS syndrome (Becker and Stoodley, 2013; Lo
430 Muzio, 2008), with cerebellar hypoplasia and reduced Purkinje cell numbers most commonly
431 linked with ASD (Bauman, 1991; Palmen et al., 2004). However, investigations mechanistically
432 linking the cerebellum to cognition and circuits modulating social behavior are preliminary and
433 deserve further attention (McKimm et al., 2014). There were no detectable differences in the
434 width of the Purkinje cell monolayer in *Ptch1*$^{+/-}$ mice or overt losses of Purkinje cells. Increases

bioRxiv preprint doi: https://doi.org/10.1101/2020.01.25.919506; this version posted January 25, 2020. The copyright holder for this preprint (which was not certified by peer review) is the author/funder, who has granted bioRxiv a license to display the preprint in perpetuity. It is made available under aCC-BY 4.0 International license.

435 in IGL area was generally evident across the entire cerebellum in both male and female *Ptch1*
436 heterozygotes, indicating that cerebellar phenotypes are likely related to increased proliferation
437 and density of granule cells that resulted in detectable increases in area of some cerebellar
438 lobules. While IGL area was generally increased across all lobules, significant cerebellar
439 overgrowth in the IGL of lobules IV/V and IX was found in both sexes, whereas GCP overgrowth
440 of lobule III reached significance in females and overgrowth of lobule VII was significant in
441 males. Lobules IV/V and IX of the cerebellum have previously been identified as sensitive to
442 SHH pathway defects via mutation of Gli1, Gli2, and Smo (Corrales et al., 2006; Tan et al.,
443 2018); both *Ptch1*$^{+/-}$ males and females developed GCP overgrowth specifically in these two
444 lobules.

445 The cerebellum is divided into functionally specific regions with lobules I-V and IX often
446 associated with motor function and working memory in rodents and humans (D'Mello et al.,
447 2015; Guell et al.; Lawrenson et al., 2018). Reductions in volume of lobules IV/V and IX are also
448 associated with social impairments in patients with autism (D'Mello et al., 2015). Vermal
449 hyperplasia of cerebellar lobules VI and VII in a subgroup of autism patients (Courchesne et al.,
450 1994), and Purkinje cell hyperplasia in lobules IV/V and IX associated with impaired social
451 behavior have been described (Cupolillo et al., 2016). Because both hypoplasia and overgrowth
452 of the different layers of the cerebellum are linked to altered social behavior, an appropriate
453 balance of Purkinje and granule cell inputs are likely necessary for normal cerebellar modulation
454 of behavior; vermal granule cell hyperplasia in *Ptch1*$^{+/-}$ females may be driving the observed
455 alterations in social behavior and hyperactivity-like phenotype.

456 Treatment for SHH MB is extremely aggressive and involves primary tumor resection
457 followed by high-dose chemotherapeutics (Kumar et al., 2017). Following treatment, behavioral
458 decrements of attention and processing speed, learning and memory, language, visual
459 perception, and executive function are common (Ribi et al., 2005). These neurological
460 complications, attributed entirely to therapeutic side effects, occur in nearly all MB survivors and

bioRxiv preprint doi: https://doi.org/10.1101/2020.01.25.919506; this version posted January 25, 2020. The copyright holder for this preprint (which was not certified by peer review) is the author/funder, who has granted bioRxiv a license to display the preprint in perpetuity. It is made available under aCC-BY 4.0 International license.

461 resemble behavioral defects and cognitive deficits observed in cerebellar-associated disorders
462 including HPE, BCNS, and William's Syndrome (Lo Muzio, 2008; Reiss et al., 2004; Weiss et
463 al., 2018b). Considering that *Ptch1*$^{+/-}$ females exhibit altered behavior, some neurological
464 complications noted in MB survivors may exist prior to treatment as disease etiology rather than
465 solely a consequence of adverse effects of treatment, and those neurological symptoms could
466 be different in males and females. Understanding of the behavioral sequelae inherent to, and
467 the innate sex differences within, MB etiology is critical to improving the treatment plan for MB
468 patients.

469 *4.3. Cerebellar modulation of social behavior*

470 Consistent with the association between reduced hippocampal size, hyperactivity, learning,
471 and memory deficits in humans (Al-Amin et al., 2018; Tamnes et al., 2014), *Ptch1*$^{+/-}$ female mice
472 exhibited changes in hippocampal structures associated with altered behavior. Altered
473 hippocampal structures have previously been reported in *Ptch1*$^{+/-}$ male mice, although females
474 were not examined (Antonelli et al., 2018). SHH signaling directs neurogenesis and is a critical
475 player in hippocampal plasticity (Yao et al., 2016). *Ptch1*$^{+/-}$ females also exhibited increased
476 cellularity and thickness of cortical layer VI.

477 Cortical layer VI is the earliest developing cortical layer (Gilmore and Herrup, 1997) and
478 has the greatest diversity of neuronal cell types, with many excitatory pyramidal neurons,
479 glutamatergic neurons, spiny stellate neurons that project to the thalamus, and local inhibitory
480 neurons (Briggs, 2010). SHH signaling is critical to mitogenesis and speciation of cortical
481 progenitors early in development (Yabut and Pleasure, 2018) and SHH signaling induces
482 cortical growth (Wang et al., 2016). The observed decrement in hippocampal size and
483 increased cortical layer thickness resulting from decreased SHH signaling provides further
484 evidence that neuronal changes outside the cerebellum may contribute to noted behavioral
485 changes in *Ptch1*$^{+/-}$ females. The observed behavioral changes in activity and social behavior
486 could be related to decreases in hippocampal plasticity and the alteration of projections to

bioRxiv preprint doi: https://doi.org/10.1101/2020.01.25.919506; this version posted January 25, 2020. The copyright holder for this preprint (which was not certified by peer review) is the author/funder, who has granted bioRxiv a license to display the preprint in perpetuity. It is made available under aCC-BY 4.0 International license.

extracerebellar circuits. Alternatively, the observed changes in cortical and hippocampal structures may result from an imbalance of extracerebellar inputs or activity to these structures resulting from the indirect influence of increased cerebellar granule cell numbers due to increased synaptic inputs on Purkinje cells and subsequent impacts on extracerebellar activity.

A potential mechanism linking abnormal cerebellar pathology to impaired social function is via cerebellar modulation of dopamine release within the mPFC (Rogers et al., 2013b). The mPFC incorporates cerebellar output through the cerebellar dentate nucleus which modulate dopamine release in the mPFC via two primary pathways that appear to contribute equally to mPFC activation: 1) contralateral glutamatergic projections from the cerebellar dentate nucleus to reticulotegmental nuclei that project to pedunculopontine nuclei and stimulate mesocortical dopaminergic neurons in the ventral tegmental area (VTA), which then project to the mPFC, or 2) contralateral glutamatergic projections of the cerebellar dentate nucleus project to thalamic mediodorsal and ventrolateral nuclei (ThN md and ThN vl) that send glutamatergic effects to the mPFC to modulate mesocortical dopaminergic terminal release in the mPFC via excitatory glutamatergic synapses (McKimm et al., 2014) (Figure 5).

Changes in projections through the VTA may explain why *Ptch1*$^{+/-}$ females display altered social behavior, because SHH is necessary for the specification of dopamine cell fate in the VTA (Blaess et al., 2011). Supporting this possibility, experimental mutation of the *Ptch* coreceptor, *Cdon* in mice, increased numbers of dopamine neurons in the VTA and eleveated levels of dopamine and its metabolites in the mPFC (Verwey et al., 2016). Thus, alterations in dopamine release within the mPFC might explain the increased activity and altered social behavior observed in female Ptch$^{+/-}$ mice. Supporting this possibility, mice with conditional inactivation of Smo specifically in dopamine cells are hyperactive (Zhou et al., 2016), whereas dopamine receptor D1 blockade in the mPFC of rats reduces the distance traveled in an open-field task (Hall et al., 2009). Those studies suggest that cerebellar-related increases in mPFC

bioRxiv preprint doi: https://doi.org/10.1101/2020.01.25.919506; this version posted January 25, 2020. The copyright holder for this preprint (which was not certified by peer review) is the author/funder, who has granted bioRxiv a license to display the preprint in perpetuity. It is made available under aCC-BY 4.0 International license.

dopamine release might mediate the alterations in activity and social observed in the *Ptch1*$^{+/-}$ females.

4.4. Female-specific effects of Ptch1 mutation

The more severe cerebellar overgrowth and behavior phenotypes observed in female *Ptch1*$^{+/-}$ mice could also be explained by increased responsiveness of GCPs to circulating estrogens. It is notable that in SHH mouse models of MB the incidence of tumors is higher in females (Svärd et al., 2009). Estrogens also play important roles in regulating cerebellar granule cell proliferation and MB progression (Guillette et al., 2018). Considering the progressive nature of MB development in *Ptch1*$^{+/-}$, the apparent increased sensitivity of females to dysregulated SHH signaling could be related to the increased levels of circulating estrogens in mature females. These activities of estrogen are mediated through modulation of rapid estrogen signaling, estrogen receptor-regulated gene expression, and resulting modulation of growth factor-related signal transduction pathways (Cookman and Belcher, 2015; Garcia-Segura et al., 2006). Increased activation of ERβ signaling increases GCP mitogenesis and migration, and upregulates neuroprotective mechanisms in mature granule cells, which also act in the etiology and progression of MB to drive tumor progression (Belcher, 2008; Cookman and Belcher, 2015; Guillette et al., 2018). It is possible that the more sever phenotypes detected in *Ptch1*$^{+/-}$ female mice are related to a relative increase in estrogen signaling in ERβ positive *Ptch1*$^{+/-}$ granule cell-like precursors. It is also possible that sex-related differences in the proposed dopaminergic cerebellar-mPFC circuitry, leading to differential dopamine release or dopamine receptor activity in the mPFC, could sex-specifically contribute to differences in structural organization and behaviors that are associated with decreased SHH signaling.

5. Conclusion

The disruption of SHH-signaling in *Ptch1*$^{+/-}$ mice causes lobule-specific overgrowth in cerebellar structures previously linked to ASD in both sexes. Additionally, *Ptch1*$^{+/-}$ mice

bioRxiv preprint doi: https://doi.org/10.1101/2020.01.25.919506; this version posted January 25, 2020. The copyright holder for this preprint (which was not certified by peer review) is the author/funder, who has granted bioRxiv a license to display the preprint in perpetuity. It is made available under aCC-BY 4.0 International license.

exhibited female-specific alterations in the hippocampus and cortical layers, hyperactivity, and altered social behaviors. Based on these findings, it is proposed that a subset of the behavioral phenotypes observed in MB patients following treatment are a component of MB sequalae rather than side effects of treatment. Further work focusing on the role of estrogen and SHH signaling cross-talk is needed to elucidate the developmental and functional nature of the proposed cerebellar-mPFC circuitry and the functional role of the cerebellum as a mediator of sex-specific behaviors.

Acknowledgements:

We are indebted to Dr. Heather Patisaul for assistance with the design and analysis of the behavioral studies, Dr. Theresa Guillette and the other members of the Belcher and Patisaul labs who assisted in various aspects of the study and gave critical feed-back on the manuscript. We would also like to express our great appreciation for the support of Sandy Elliott and the staff of the NCSU BRF who go above and beyond to facilitate our animal studies.

bioRxiv preprint doi: https://doi.org/10.1101/2020.01.25.919506; this version posted January 25, 2020. The copyright holder for this preprint (which was not certified by peer review) is the author/funder, who has granted bioRxiv a license to display the preprint in perpetuity. It is made available under aCC-BY 4.0 International license.

Figure Legend

Figure 1. Behavioral assessment using a novel open-field task. Maximum velocity (A), total distance traveled (B), and distance traveled over 5-min periods in females (C) and males (D) are shown. Values are expressed as mean ± SEM. * = $p < .05$. Final animal numbers animals used for novel social task follow. Females: wild-type, n=18; *Ptch1*$^{+/-}$, n=18. Males: wild-type, n=23; *Ptch1*$^{+/-}$, n=13. Three wild-type females were excluded because they climbed atop the holding cup and avoided the task.

Figure 2. Behavioral assessment using a partner preference task. Duration of interactions with novel and familiar animals (A), the number of those interactions (B), and the type of those interactions (C) are shown. Lower-cased (a) and (b) illustrate significant differences within each level of the ANOVA compared to wild-type females. Values are expressed as mean ± SEM. * = $p < .05$. Final animal numbers animals used for partner preference task follow. Females: wild-type, n=17; *Ptch1*$^{+/-}$, n=14. Males: wild-type, n=19; *Ptch1*$^{+/-}$, n=12. One wild-type female that climbed atop the holding cup and avoided performing the task was excluded.

Figure 3. Assessment of changes in cerebellar structures. Sagittal cerebellar section (20 μm) showing lobular definition in a Wild-Type female, with cerebellar lobules (II – X) and the fourth ventricle labeled (V4). The lobular structures are outlined as quantified (A). The hatched outline in (A) denotes the region compared to a *Ptch1*$^{+/-}$ female (B), where differences in *Ptch1*$^{+/-}$ females are highlighted with an arrow indicating ectopic overgrowth and asterisks showing overgrowth of lobule IX (B). A wild-type male (C) and *Ptch1*$^{+/-}$ male (D) are also shown. Individual lobular IGL area are shown (E). Scale bar = 1 mm. Values are expressed as mean ± SEM. * = $p < .05$. Final animal numbers animals used for IGL area comparison follow. Females: wild-type, n=9; *Ptch1*$^{+/-}$, n=5. Males: wild-type, n=9; *Ptch1*$^{+/-}$, n=9.

bioRxiv preprint doi: https://doi.org/10.1101/2020.01.25.919506; this version posted January 25, 2020. The copyright holder for this preprint (which was not certified by peer review) is the author/funder, who has granted bioRxiv a license to display the preprint in perpetuity. It is made available under aCC-BY 4.0 International license.

Figure 4. Assessment of changes in cortical structures. Coronal brain section (40 μm) highlighting measured regions of cortex (CTX), ammon's horn (CA1, CA3), dentate gyrus (DG) (A) with region identified using caudate putamen (CP) and thalamus (TH) as landmarks. Inset image shows cortical layers (labeled I, II-IV, V, and VI of WT female (B) and *Ptch*$^{+/-}$ female mouse (C). Ammon's horn (CA1-3), dentate gyrus, and cerebral cortex are outlined in red. Cortical layers are labeled I, II-IV, V, and VI. Scale bar = 1 mm (A) and 500 μm (B,C). Expressed as mean ± SEM. * = $p < .05$. For overall cortical layer length and width, the number of analyzed animals follow. Females: wild-type, n=4; *Ptch1*$^{+/-}$, n=4. Males: wild-type, n=6; *Ptch1*$^{+/-}$, n=4. Final animal numbers for individual cortical layers follow. Females: wild-type, n=4; *Ptch1*$^{+/-}$, n=3. Males: wild-type, n=6; *Ptch1*$^{+/-}$, n=3.

Figure 5. Proposed pathway of cerebello-cortical circuitry. Shown is a cartoon of the proposed neuronal circuits linking outputs from the cerebellar cortex (CBX) to projections from deep cerebellar nuclei (DN) to neurons in the prefrontal cortex (PFC) via the tegmental reticular nuclei (TRN), pedunculopontine nuclei (PPN), the ventral tegmental area (VTA), thalamic mediodorsal (MD) and ventrolateral (VL) nuclei, and pontine reticular nuclei (PRN).

bioRxiv preprint doi: https://doi.org/10.1101/2020.01.25.919506; this version posted January 25, 2020. The copyright holder for this preprint (which was not certified by peer review) is the author/funder, who has granted bioRxiv a license to display the preprint in perpetuity. It is made available under aCC-BY 4.0 International license.

589 **References:**

590 Al-Amin, M., Zinchenko, A., and Geyer, T. (2018). Hippocampal subfield volume
591 changes in subtypes of attention deficit hyperactivity disorder. Brain Res. *1685*, 1–8.

592 Altman, J., and Bayer, S.A. (1997). Development of the cerebellar system: in relation to
593 its evolution, structure, and functions (CRC Press).

594 Antonelli, F., Casciati, A., Tanori, M., Tanno, B., Linares-Vidal, M.V., Serra, N., Bellés,
595 M., Pannicelli, A., Saran, A., and Pazzaglia, S. (2018). Alterations in Morphology and
596 Adult Neurogenesis in the Dentate Gyrus of Patched1 Heterozygous Mice. Front. Mol.
597 Neurosci. *11*.

598 Bailey, K.R., and Crawley, J.N. (2009). Anxiety-Related Behaviors in Mice. In Methods
599 of Behavior Analysis in Neuroscience, J.J. Buccafusco, ed. (Boca Raton (FL): CRC
600 Press/Taylor & Francis), p.

601 Bauman, M.L. (1991). Microscopic neuroanatomic abnormalities in autism. Pediatrics
602 *87*, 791–796.

603 Becker, E.B.E., and Stoodley, C.J. (2013). Autism spectrum disorder and the
604 cerebellum. Int. Rev. Neurobiol. *113*, 1–34.

605 Belcher, S.M. (2008). Rapid signaling mechanisms of estrogens in the developing
606 cerebellum. Brain Res. Rev. *57*, 481–492.

607 Blaess, S., Bodea, G.O., Kabanova, A., Chanet, S., Mugniery, E., Derouiche, A.,
608 Stephen, D., and Joyner, A.L. (2011). Temporal-spatial changes in Sonic Hedgehog
609 expression and signaling reveal different potentials of ventral mesencephalic
610 progenitors to populate distinct ventral midbrain nuclei. Neural Develop. *6*, 29.

611 Briggs, F. (2010). Organizing Principles of Cortical Layer 6. Front. Neural Circuits *4*.

612 Cookman, C.J., and Belcher, S.M. (2015). Estrogen Receptor-β Up-Regulates IGF1R
613 Expression and Activity to Inhibit Apoptosis and Increase Growth of Medulloblastoma.
614 Endocrinology *156*, 2395–2408.

615 Corrales, J.D., Blaess, S., Mahoney, E.M., and Joyner, A.L. (2006). The level of sonic
616 hedgehog signaling regulates the complexity of cerebellar foliation. Dev. Camb. Engl.
617 *133*, 1811–1821.

618 Courchesne, E., Saitoh, O., Yeung-Courchesne, R., Press, G.A., Lincoln, A.J., Haas,
619 R.H., and Schreibman, L. (1994). Abnormality of cerebellar vermian lobules VI and VII
620 in patients with infantile autism: identification of hypoplastic and hyperplastic subgroups
621 with MR imaging. AJR Am. J. Roentgenol. *162*, 123–130.

622 Croen, L.A., Shaw, G.M., and Lammer, E.J. (1996). Holoprosencephaly: epidemiologic
623 and clinical characteristics of a California population. Am. J. Med. Genet. *64*, 465–472.

bioRxiv preprint doi: https://doi.org/10.1101/2020.01.25.919506; this version posted January 25, 2020. The copyright holder for this preprint (which was not certified by peer review) is the author/funder, who has granted bioRxiv a license to display the preprint in perpetuity. It is made available under aCC-BY 4.0 International license.

624 Cupolillo, D., Hoxha, E., Faralli, A., De Luca, A., Rossi, F., Tempia, F., and Carulli, D.
625 (2016). Autistic-Like Traits and Cerebellar Dysfunction in Purkinje Cell *PTEN* Knock-Out
626 Mice. Neuropsychopharmacology *41*, 1457–1466.

627 Dahmane, N., and Ruiz i Altaba, A. (1999). Sonic hedgehog and cerebellum
628 development. 12.

629 Daynac, M., Tirou, L., Faure, H., Mouthon, M.-A., Gauthier, L.R., Hahn, H., Boussin,
630 F.D., and Ruat, M. (2016). Hedgehog Controls Quiescence and Activation of Neural
631 Stem Cells in the Adult Ventricular-Subventricular Zone. Stem Cell Rep. *7*, 735–748.

632 Dey, J., Ditzler, S., Knoblaugh, S.E., Hatton, B.A., Schelter, J.M., Cleary, M.A.,
633 Mecham, B., Rorke-Adams, L.B., and Olson, J.M. (2012). A Distinct Smoothened
634 Mutation Causes Severe Cerebellar Developmental Defects and Medulloblastoma in a
635 Novel Transgenic Mouse Model. Mol. Cell. Biol. *32*, 4104–4115.

636 D'Mello, A.M., Crocetti, D., Mostofsky, S.H., and Stoodley, C.J. (2015). Cerebellar gray
637 matter and lobular volumes correlate with core autism symptoms. NeuroImage Clin. *7*,
638 631–639.

639 Dutka, T., Hallberg, D., and Reeves, R.H. (2015). Chronic up-regulation of the SHH
640 pathway normalizes some developmental effects of trisomy in Ts65Dn mice. Mech.
641 Dev. *0*, 68–80.

642 Garcia-Segura, L.M., Sanz, A., and Mendez, P. (2006). Cross-talk between IGF-I and
643 estradiol in the brain: focus on neuroprotection. Neuroendocrinology *84*, 275–279.

644 Gilmore, E.C., and Herrup, K. (1997). Cortical development: Layers of complexity. Curr.
645 Biol. *7*, R231–R234.

646 Gloude, N.J., Yoon, J.M., and Crawford, J.R. (2016). Novel PTCH1 Mutation in a Young
647 Child With Gorlin Syndrome and Medulloblastoma. Pediatr. Blood Cancer *63*, 1128–
648 1129.

649 Gomez, H.G., Noguchi, H., Castillo, J.G., Aguilar, D., Pleasure, S.J., and Yabut, O.R.
650 (2019). Suppressor of Fused regulates the proliferation of postnatal neural stem and
651 precursor cells via a Gli3-dependent mechanism. Biol. Open *8*.

652 Goodrich, L.V., Milenković, L., Higgins, K.M., and Scott, M.P. (1997). Altered neural cell
653 fates and medulloblastoma in mouse patched mutants. Science *277*, 1109–1113.

654 Grammel, D., Warmuth-Metz, M., von Bueren, A.O., Kool, M., Pietsch, T., Kretzschmar,
655 H.A., Rowitch, D.H., Rutkowski, S., Pfister, S.M., and Schüller, U. (2012). Sonic
656 hedgehog-associated medulloblastoma arising from the cochlear nuclei of the
657 brainstem. Acta Neuropathol. (Berl.) *123*, 601–614.

658 Guell, X., Schmahmann, J.D., Gabrieli, J.D., and Ghosh, S.S. Functional gradients of
659 the cerebellum. ELife *7*.

bioRxiv preprint doi: https://doi.org/10.1101/2020.01.25.919506; this version posted January 25, 2020. The copyright holder for this preprint (which was not certified by peer review) is the author/funder, who has granted bioRxiv a license to display the preprint in perpetuity. It is made available under aCC-BY 4.0 International license.

660 Guillette, T.C., Jackson, T.W., and Belcher, S.M. (2018). Duality of estrogen receptor β
661 action in cancer progression. Curr. Opin. Pharmacol. *41*, 66–73.

662 Hahn, H., Wicking, C., Zaphiropoulos, P.G., Gailani, M.R., Shanley, S., Chidambaram,
663 A., Vorechovsky, I., Holmberg, E., Unden, A.B., Gillies, S., et al. (1996). Mutations of
664 the Human Homolog of Drosophila patched in the Nevoid Basal Cell Carcinoma
665 Syndrome. Cell *85*, 841–851.

666 Haldipur, P., Bharti, U., Govindan, S., Sarkar, C., Iyengar, S., Gressens, P., and Mani,
667 S. (2011). Expression of Sonic Hedgehog During Cell Proliferation in the Human
668 Cerebellum. Stem Cells Dev. *21*, 1059–1068.

669 Hall, D.A., Powers, J.P., and Gulley, J.M. (2009). Blockade of D1 dopamine receptors in
670 the medial prefrontal cortex attenuates amphetamine- and methamphetamine-induced
671 locomotor activity in the rat. Brain Res. *1300*, 51–57.

672 Hallahan, A.R., Pritchard, J.I., Hansen, S., Benson, M., Stoeck, J., Hatton, B.A.,
673 Russell, T.L., Ellenbogen, R.G., Bernstein, I.D., Beachy, P.A., et al. (2004). The SmoA1
674 Mouse Model Reveals That Notch Signaling Is Critical for the Growth and Survival of
675 Sonic Hedgehog-Induced Medulloblastomas. Cancer Res. *64*, 7794–7800.

676 Heussler, H., Suri, M., Young, I., and Muenke, M. (2002). Extreme variability of
677 expression of a Sonic Hedgehog mutation: attention difficulties and holoprosencephaly.
678 Arch. Dis. Child. *86*, 293–296.

679 Ihrie, R.A., Shah, J.K., Harwell, C.C., Levine, J.H., Guinto, C.D., Lezameta, M.,
680 Kriegstein, A.R., and Alvarez-Buylla, A. (2011). Persistent sonic hedgehog signaling in
681 adult brain determines neural stem cell positional identity. Neuron *71*, 250–262.

682 Jakab, R.L., Wong, J.K., and Belcher, S.M. (2001). Estrogen receptor beta
683 immunoreactivity in differentiating cells of the developing rat cerebellum. J. Comp.
684 Neurol. *430*, 396–409.

685 Kumar, V., Kumar, V., McGuire, T., Coulter, D.W., Sharp, J.G., and Mahato, R.I. (2017).
686 Challenges and Recent Advances in Medulloblastoma Therapy. Trends Pharmacol. Sci.
687 *38*, 1061–1084.

688 Lacombe, D., Chateil, J.F., Fontan, D., and Battin, J. (1990). Medulloblastoma in the
689 nevoid basal-cell carcinoma syndrome: case reports and review of the literature. Genet.
690 Couns. Geneva Switz. *1*, 273–277.

691 Lawrenson, C., Bares, M., Kamondi, A., Kovács, A., Lumb, B., Apps, R., Filip, P., and
692 Manto, M. (2018). The mystery of the cerebellum: clues from experimental and clinical
693 observations. Cerebellum Ataxias *5*.

694 Lee, Y., Kawagoe, R., Sasai, K., Li, Y., Russell, H.R., Curran, T., and McKinnon, P.J.
695 (2007). Loss of suppressor-of-fused function promotes tumorigenesis. Oncogene *26*,
696 6442–6447.

bioRxiv preprint doi: https://doi.org/10.1101/2020.01.25.919506; this version posted January 25, 2020. The copyright holder for this preprint (which was not certified by peer review) is the author/funder, who has granted bioRxiv a license to display the preprint in perpetuity. It is made available under aCC-BY 4.0 International license.

Lo Muzio, L. (2008). Nevoid basal cell carcinoma syndrome (Gorlin syndrome). Orphanet J. Rare Dis. *3*, 32.

Martinez, S., Andreu, A., Mecklenburg, N., and Echevarria, D. (2013). Cellular and molecular basis of cerebellar development. Front. Neuroanat. *7*.

McKimm, E., Corkill, B., Goldowitz, D., Albritton, L.M., Homayouni, R., Blaha, C.D., and Mittleman, G. (2014). Glutamate dysfunction associated with developmental cerebellar damage: relevance to autism spectrum disorders. Cerebellum Lond. Engl. *13*, 346–353.

Ming, J.E., Kaupas, M.E., Roessler, E., Brunner, H.G., Golabi, M., Tekin, M., Stratton, R.F., Sujansky, E., Bale, S.J., and Muenke, M. (2002). Mutations in PATCHED-1, the receptor for SONIC HEDGEHOG, are associated with holoprosencephaly. Hum. Genet. *110*, 297–301.

Mouden, C., Dubourg, C., Carré, W., Rose, S., Quelin, C., Akloul, L., Hamdi-Rozé, H., Viot, G., Salhi, H., Darnault, P., et al. (2016). Complex mode of inheritance in holoprosencephaly revealed by whole exome sequencing. Clin. Genet. *89*, 659–668.

Nanni, L., Ming, J.E., Bocian, M., Steinhaus, K., Bianchi, D.W., Die-Smulders, C., Giannotti, A., Imaizumi, K., Jones, K.L., Campo, M.D., et al. (1999). The mutational spectrum of the sonic hedgehog gene in holoprosencephaly: SHH mutations cause a significant proportion of autosomal dominant holoprosencephaly. Hum. Mol. Genet. *8*, 2479–2488.

Nitzki, F., Becker, M., Frommhold, A., Schulz-Schaeffer, W., and Hahn, H. (2012). Patched Knockout Mouse Models of Basal Cell Carcinoma. J. Skin Cancer *2012*.

Northcott, P.A., Dubuc, A.M., Pfister, S., and Taylor, M.D. (2012). Molecular subgroups of medulloblastoma. Expert Rev. Neurother. *12*, 871–884.

Okamoto, N., Naruto, T., Kohmoto, T., Komori, T., and Imoto, I. (2014). A novel PTCH1 mutation in a patient with Gorlin syndrome. Hum. Genome Var. *1*, 14022.

Palmen, S.J.M.C., van Engeland, H., Hof, P.R., and Schmitz, C. (2004). Neuropathological findings in autism. Brain J. Neurol. *127*, 2572–2583.

Phillips, J.R., Hewedi, D.H., Eissa, A.M., and Moustafa, A.A. (2015). The Cerebellum and Psychiatric Disorders. Front. Public Health *3*.

Rahimi-Balaei, M., Bergen, H., Kong, J., and Marzban, H. (2018). Neuronal Migration During Development of the Cerebellum. Front. Cell. Neurosci. *12*.

Reiss, A.L., Eckert, M.A., Rose, F.E., Karchemskiy, A., Kesler, S., Chang, M., Reynolds, M.F., Kwon, H., and Galaburda, A. (2004). An Experiment of Nature: Brain Anatomy Parallels Cognition and Behavior in Williams Syndrome. J. Neurosci. Off. J. Soc. Neurosci. *24*, 5009–5015.

bioRxiv preprint doi: https://doi.org/10.1101/2020.01.25.919506; this version posted January 25, 2020. The copyright holder for this preprint (which was not certified by peer review) is the author/funder, who has granted bioRxiv a license to display the preprint in perpetuity. It is made available under aCC-BY 4.0 International license.

Ribi, K., Relly, C., Landolt, M.A., Alber, F.D., Boltshauser, E., and Grotzer, M.A. (2005). Outcome of medulloblastoma in children: long-term complications and quality of life. Neuropediatrics *36*, 357–365.

Rogers, T.D., McKimm, E., Dickson, P.E., Goldowitz, D., Blaha, C.D., and Mittleman, G. (2013a). Is autism a disease of the cerebellum? An integration of clinical and pre-clinical research. Front. Syst. Neurosci. *7*.

Rogers, T.D., Dickson, P.E., McKimm, E., Heck, D.H., Goldowitz, D., Blaha, C.D., and Mittleman, G. (2013b). Reorganization of circuits underlying cerebellar modulation of prefrontal cortical dopamine in mouse models of autism spectrum disorder. Cerebellum Lond. Engl. *12*.

Schüller, U., Heine, V.M., Mao, J., Kho, A.T., Dillon, A.K., Han, Y.-G., Huillard, E., Sun, T., Ligon, A.H., Qian, Y., et al. (2008). Acquisition of Granule Neuron Precursor Identity Is a Critical Determinant of Progenitor Cell Competence to Form Shh-Induced Medulloblastoma. Cancer Cell *14*, 123–134.

Shiohama, T., Fujii, K., Miyashita, T., Mizuochi, H., Uchikawa, H., and Shimojo, N. (2017). Brain morphology in children with nevoid basal cell carcinoma syndrome. Am. J. Med. Genet. A. *173*, 946–952.

Silverman, J.L., Yang, M., Lord, C., and Crawley, J.N. (2010). Behavioural phenotyping assays for mouse models of autism. Nat. Rev. Neurosci. *11*, 490–502.

Solomon, B.D., Mercier, S., Vélez, J.I., Pineda-Alvarez, D.E., Wyllie, A., Zhou, N., Dubourg, C., David, V., Odent, S., Roessler, E., et al. (2010). Analysis of Genotype-Phenotype Correlations in Human Holoprosencephaly. Am. J. Med. Genet. C Semin. Med. Genet. *154C*, 133–141.

Solomon, B.D., Pineda-Alvarez, D.E., Gropman, A.L., Willis, M.J., Hadley, D.W., and Muenke, M. (2012). High Intellectual Function in Individuals with Mutation-Positive Microform Holoprosencephaly. Mol. Syndromol. *3*, 140–142.

Sun, T., Plutynski, A., Ward, S., and Rubin, J.B. (2015). An integrative view on sex differences in brain tumors. Cell. Mol. Life Sci. *72*, 3323–3342.

Svärd, J., Rozell, B., Toftgård, R., and Teglund, S. (2009). Tumor suppressor gene co-operativity in compound Patched1 and Suppressor of fused heterozygous mutant mice. Mol. Carcinog. *48*, 408–419.

Tamnes, C.K., Walhovd, K.B., Engvig, A., Grydeland, H., Krogsrud, S.K., stby, Y., Holland, D., Dale, A.M., and Fjell, A.M. (2014). Regional Hippocampal Volumes and Development Predict Learning and Memory. Dev. Neurosci. *36*, 161–174.

Tan, I.-L., Wojcinski, A., Rallapalli, H., Lao, Z., Sanghrajka, R.M., Stephen, D., Volkova, E., Korshunov, A., Remke, M., Taylor, M.D., et al. (2018). Lateral cerebellum is

bioRxiv preprint doi: https://doi.org/10.1101/2020.01.25.919506; this version posted January 25, 2020. The copyright holder for this preprint (which was not certified by peer review) is the author/funder, who has granted bioRxiv a license to display the preprint in perpetuity. It is made available under aCC-BY 4.0 International license.

768 preferentially sensitive to high sonic hedgehog signaling and medulloblastoma
769 formation. Proc. Natl. Acad. Sci. *115*, 3392–3397.

770 Tong, C.K., Fuentealba, L.C., Shah, J.K., Lindquist, R.A., Ihrie, R.A., Guinto, C.D.,
771 Rodas-Rodriguez, J.L., and Alvarez-Buylla, A. (2015). A Dorsal SHH-Dependent
772 Domain in the V-SVZ Produces Large Numbers of Oligodendroglial Lineage Cells in the
773 Postnatal Brain. Stem Cell Rep. *5*, 461–470.

774 Turner, A.H., Greenspan, K.S., and van Erp, T.G.M. (2016). Pallidum and lateral
775 ventricle volume enlargement in autism spectrum disorder. Psychiatry Res.
776 Neuroimaging *252*, 40–45.

777 Uziel, T. (2005). The tumor suppressors Ink4c and p53 collaborate independently with
778 Patched to suppress medulloblastoma formation. Genes Dev. *19*, 2656–2667.

779 Verwey, M., Grant, A., Meti, N., Adye-White, L., Torres-Berrío, A., Rioux, V., Lévesque,
780 M., Charron, F., and Flores, C. (2016). Mesocortical Dopamine Phenotypes in Mice
781 Lacking the Sonic Hedgehog Receptor Cdon. ENeuro *3*.

782 Wang, L., Hou, S., and Han, Y.-G. (2016). Hedgehog signaling promotes basal
783 progenitor expansion and the growth and folding of the neocortex. Nat. Neurosci. *19*,
784 888–896.

785 Weiss, K., Kruszka, P., Guillen Sacoto, M.J., Addissie, Y.A., Hadley, D.W., Hadsall,
786 C.K., Stokes, B., Hu, P., Roessler, E., Solomon, B., et al. (2018a). In-depth
787 investigations of adolescents and adults with holoprosencephaly identify unique
788 characteristics. Genet. Med. *20*, 14–23.

789 Weiss, K., Kruszka, P.S., Levey, E., and Muenke, M. (2018b). Holoprosencephaly from
790 conception to adulthood. Am. J. Med. Genet. C Semin. Med. Genet. *178*, 122–127.

791 Wetmore, C., Eberhart, D.E., and Curran, T. (2001). Loss of p53 but not ARF
792 Accelerates Medulloblastoma in Mice Heterozygous for patched. Cancer Res. *61*, 513–
793 516.

794 Winslow, J.T. (2003). Mouse Social Recognition and Preference. Curr. Protoc.
795 Neurosci. *22*, 8.16.1-8.16.16.

796 Yabut, O.R., and Pleasure, S.J. (2018). Sonic Hedgehog Signaling Rises to the
797 Surface: Emerging Roles in Neocortical Development. Brain Plast. *3*, 119–128.

798 Yang, M., and Crawley, J.N. (2009). Simple Behavioral Assessment of Mouse Olfaction.
799 Curr. Protoc. Neurosci. *48*, 8.24.1-8.24.12.

800 Yao, P.J., Petralia, R.S., and Mattson, M.P. (2016). Sonic Hedgehog Signaling and
801 Hippocampal Neuroplasticity. Trends Neurosci. *39*, 840–850.

bioRxiv preprint doi: https://doi.org/10.1101/2020.01.25.919506; this version posted January 25, 2020. The copyright holder for this preprint (which was not certified by peer review) is the author/funder, who has granted bioRxiv a license to display the preprint in perpetuity. It is made available under aCC-BY 4.0 International license.

802 Zhou, X., Pace, J., Filichia, E., Lv, T., Davis, B., Hoffer, B., Selman, W., and Luo, Y.
803 (2016). Effect of the sonic hedgehog receptor smoothened on the survival and function
804 of dopaminergic neurons. Exp. Neurol. *283*, 235–245.

805 Zurawel, R.H., Allen, C., Wechsler-Reya, R., Scott, M.P., and Raffel, C. (2000).
806 Evidence that haploinsufficiency of Ptch leads to medulloblastoma in mice. Genes.
807 Chromosomes Cancer *28*, 77–81.

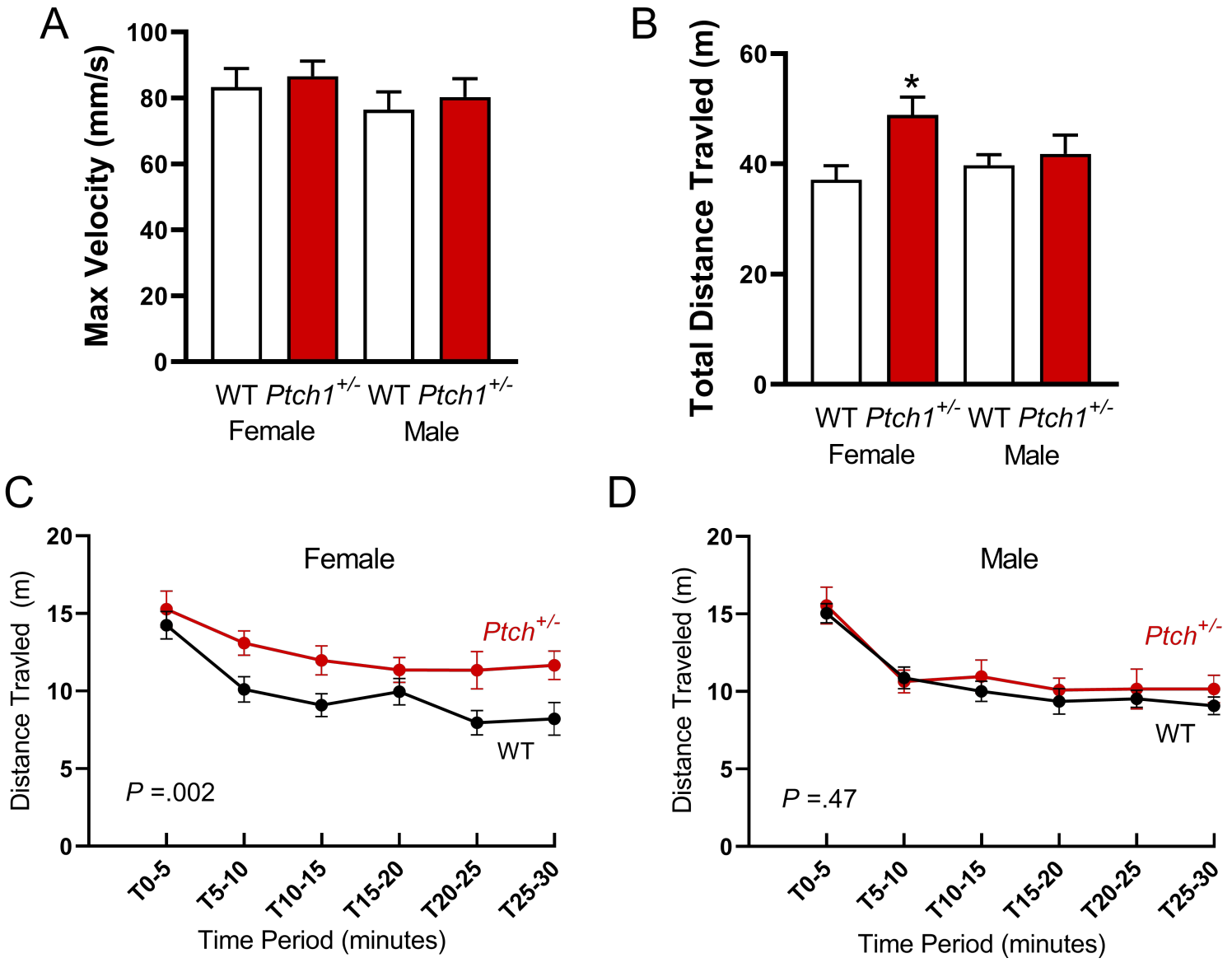
A
Max Velocity (mm/s)
100
80
60
40
20
0
WT Ptch1+/-
Female
WT Ptch1+/-
Male
B
Total Distance Travled (m)
60
40
20
0
*
WT Ptch1+/-
Female
WT Ptch1+/-
Male
C
Female
Distance Travled (m)
20
15
10
5
0
Ptch+/-
WT
P =.002
T0-5
T5-10
T10-15
T15-20
T20-25
T25-30
Time Period (minutes)
D
Male
Distance Traveled (m)
20
15
10
5
0
Ptch+/-
WT
P =.47
T0-5
T5-10
T10-15
T15-20
T20-25
T25-30
Time Period (minutes)

bioRxiv preprint doi: https://doi.org/10.1101/2020.01.25.919506; this version posted January 25, 2020. The copyright holder for this preprint (which was not certified by peer review) is the author/funder, who has granted bioRxiv a license to display the preprint in perpetuity. It is made available under aCC-BY 4.0 International license.

A

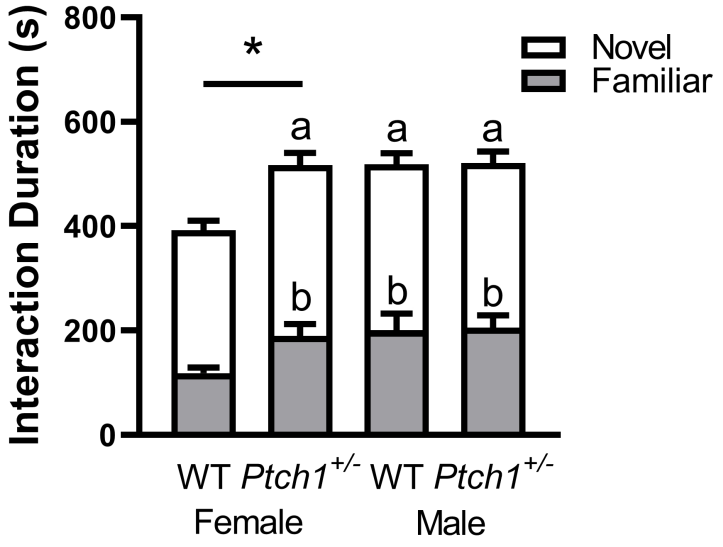

B

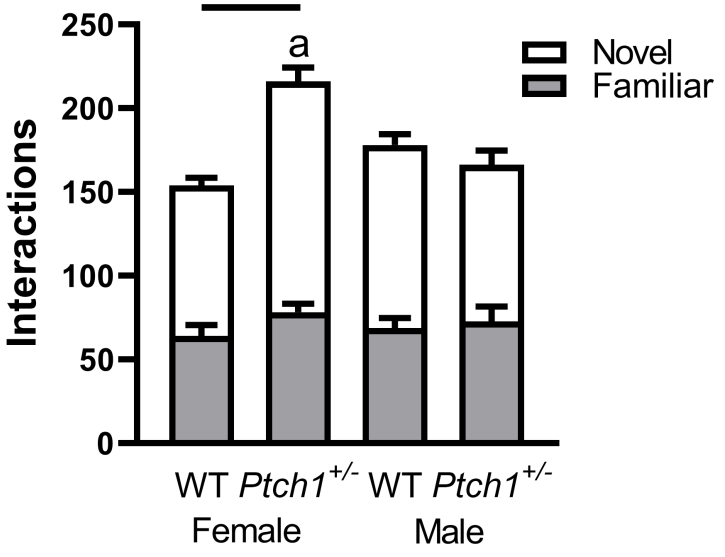

C

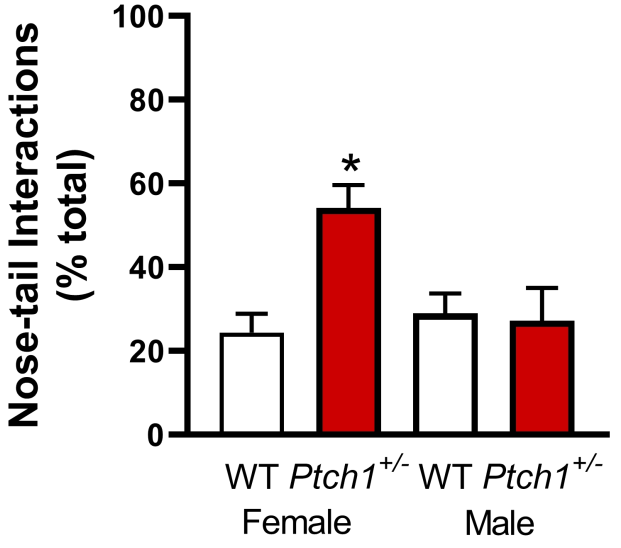

bioRxiv preprint doi: https://doi.org/10.1101/2020.01.25.919506; this version posted January 25, 2020. The copyright holder for this preprint (which was not certified by peer review) is the author/funder, who has granted bioRxiv a license to display the preprint in perpetuity. It is made available under aCC-BY 4.0 International license.

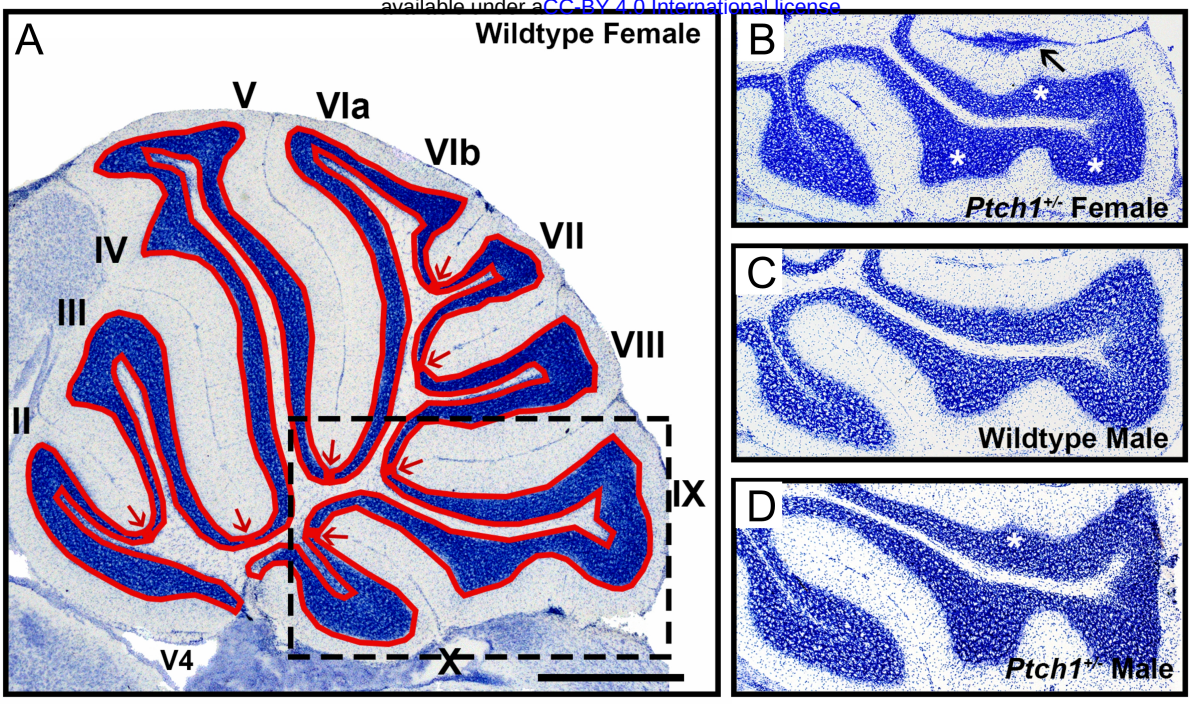

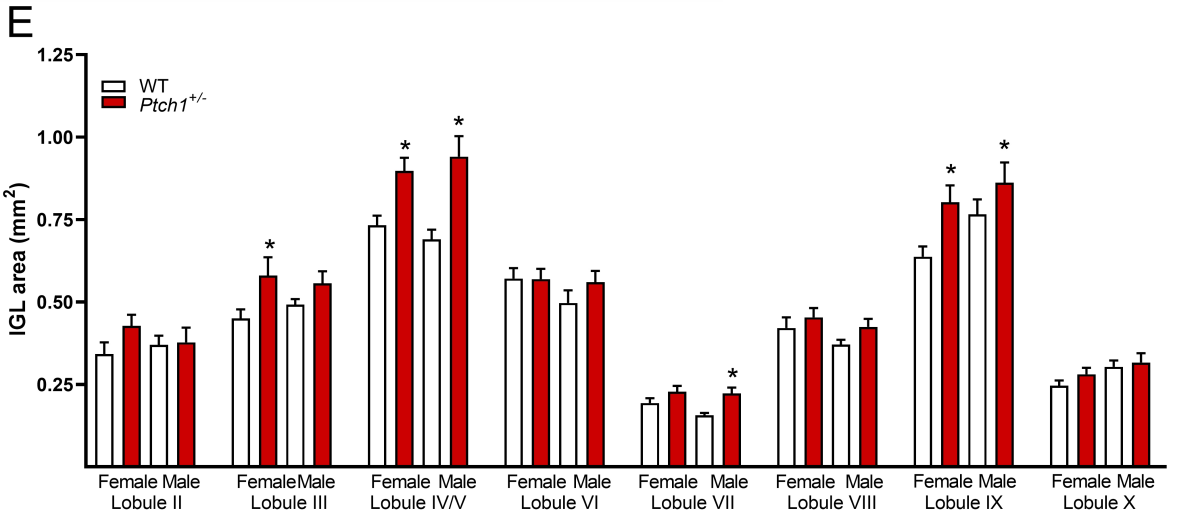

bioRxiv preprint doi: https://doi.org/10.1101/2020.01.25.919506; this version posted January 25, 2020. The copyright holder for this preprint (which was not certified by peer review) is the author/funder, who has granted bioRxiv a license to display the preprint in perpetuity. It is made available under aCC-BY 4.0 International license.

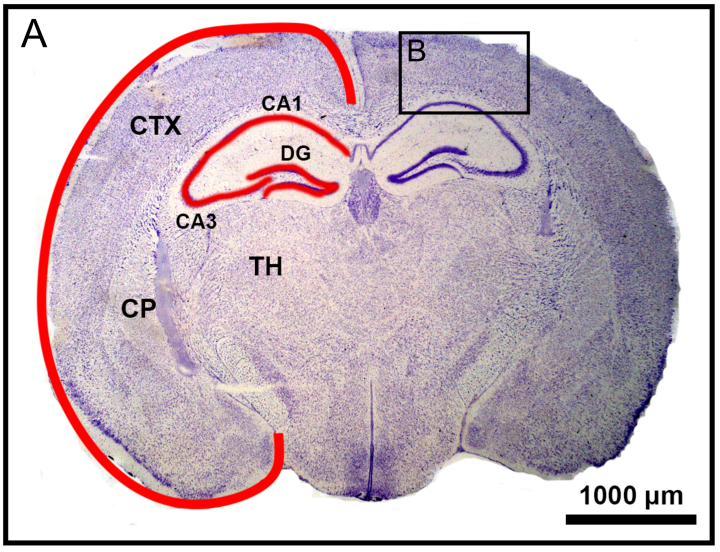

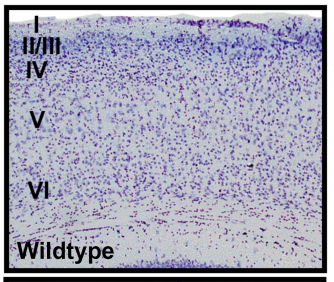

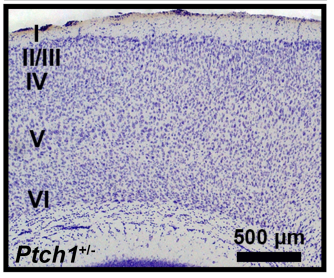

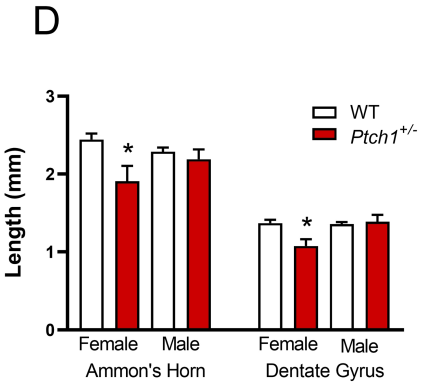

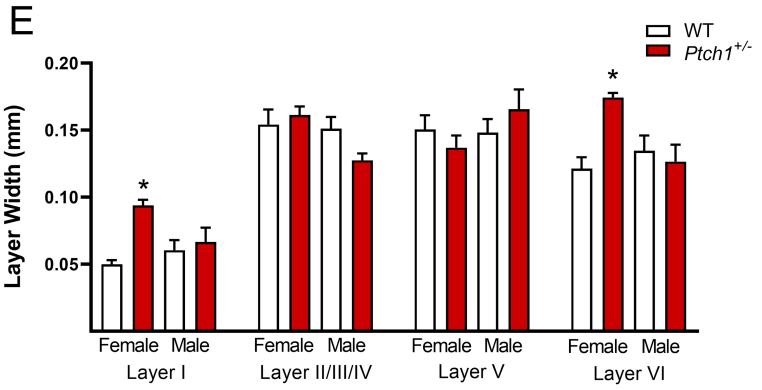

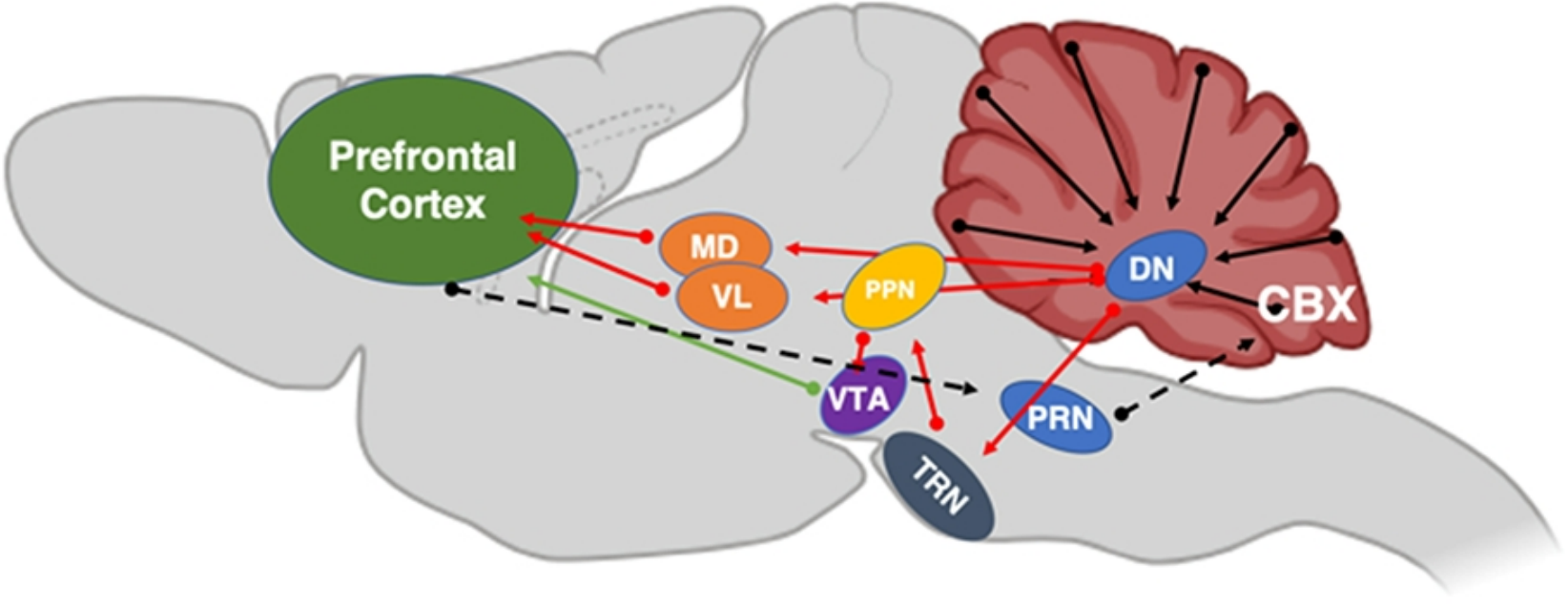
Prefrontal Cortex
MD
VL
PPN
DN
CBX
VTA
PRN
TRN

bioRxiv preprint doi: https://doi.org/10.1101/2020.01.25.919506; this version posted January 25, 2020. The copyright holder for this preprint (which was not certified by peer review) is the author/funder, who has granted bioRxiv a license to display the preprint in perpetuity. It is made available under aCC-BY 4.0 International license.

Table 1. Internal Granule Cell Layer Area

	Wild-Type	*Ptch1*$^{+/-}$	Wild-Type	*Ptch1*$^{+/-}$
Lobule	**Female**		**Male**	
II	0.342 ± 0.035	0.427 ± 0.033	0.369 ± 0.028	0.377 ± 0.044
III	0.450 ± 0.027	0.580 ± 0.055	0.492 ± 0.017	0.556 ± 0.037
IV/V	0.732 ± 0.029	**0.897 ± 0.040***	0.690 ± 0.029	**0.941 ± 0.062***
VI	0.570 ± 0.031	0.569 ± 0.031	0.468 ± 0.034	**0.616 ± 0.046***
VII	0.193 ± 0.015	**0.227 ± 0.018***	0.156 ± 0.007	**0.222 ± 0.017***
VIII	0.421 ± 0.032	**0.453 ± 0.028***	0.371 ± 0.015	**0.424 ± 0.024***
IX	0.637 ± 0.031	**0.803 ± 0.051***	0.765 ± 0.045	**0.861 ± 0.061***
X	0.246 ± 0.015	0.280 ± 0.019	0.303 ± 0.019	0.316 ± 0.028

Measurements expressed as mean ± SEM (mm^2). * = $p < .05$.